International Conference on Space Optics—ICSO 2014

La Caleta, Tenerife, Canary Islands

7–10 October 2014

Edited by Zoran Sodnik, Bruno Cugny, and Nikos Karafolas

Heating of large format filters in sub-mm and fir space optics

N. Baccichet

G. Savini

International Conference on Space Optics — ICSO 2014, edited by Zoran Sodnik, Nikos Karafolas, Bruno Cugny, Proc. of SPIE Vol. 10563, 105635R · © 2014 ESA and CNES
CCC code: 0277-786X/17/$18 · doi: 10.1117/12.2304134

HEATING OF LARGE FORMAT FILTERS IN SUB-MM AND FIR SPACE OPTICS

N. Baccichet[1], G. Savini[1]
[1]*University College London, Department of Physics and Astronomy, Gower Place, London WC1E 6BT United Kingdom*

ABSTRACT

Most FIR and sub-mm space borne observatories use polymer-based quasi-optical elements like filters and lenses, due to their high transparency and low absorption in such wavelength ranges. Nevertheless, data from those missions have proven that thermal imbalances in the instrument (not caused by filters) can complicate the data analysis. Consequently, for future, higher precision instrumentation, further investigation is required on any thermal imbalances embedded in such polymer-based filters.
Particularly, in this paper the heating of polymers when operating at cryogenic temperature in space will be studied. Such phenomenon is an important aspect of their functioning since the transient emission of unwanted thermal radiation may affect the scientific measurements. To assess this effect, a computer model was developed for polypropylene based filters and PTFE-based coatings. Specifically, a theoretical model of their thermal properties was created and used into a multi-physics simulation that accounts for conductive and radiative heating effects of large optical elements, the geometry of which was suggested by the large format array instruments designed for future space missions.
It was found that in the simulated conditions, the filters temperature was characterized by a time-dependent behaviour, modulated by a small scale fluctuation. Moreover, it was noticed that thermalization was reached only when a low power input was present.

I. INTRODUCTION

Recently, with the successful conclusion of the ESA missions Herschel [1] and Planck [2] important lessons were learned on the amount of data analysis required to extract the astrophysical signal from the raw one. At the same time preliminary designs of the successors of such missions such as SPICA [3] and the next generation CMB experiments have begun[4-6], which unavoidably brings up the question on how to increase their performances of at least one order of magnitude better that their predecessors. One of the issues that arise is the potential heating of band-defining and heat-rejecting filters [7, 8]. In this case, the thermal model applied to the data do not show an appreciable [9] signal variation, but instrument behaviour in some cases empirically fit, suggest that all thermal related effects should be understood, so as to simplify the data reduction chain of future instrument, since the wider the aperture stop, the higher the risk of such an issue.
Moreover, the basic component of such filters (polypropylene) is known to be mostly transparent in the far-infrared and sub-millimetre, but highly absorbing in the near and mid-infrared which, combined with the minimal emission in the band of detection, causes these filters to behave as transducers of NIR power into FIR power.

A possible solution to such effect in band defining filters, has been designed for present and future ground-based instrument and consists of adapting micro-strip filters on the detector itself. On the other hand, thermal rejection is still delegated to thin film interference filters, the performances of which are likely to improve in the future, raising their effectiveness, but at present no FIR satellite design has been devoid of quasi-optical components.

This paper focuses on the filters employed in large format array instruments for a next-generation CMB spacecraft with an observation mode similar to the Planck one, as shown in section 2. Particularly, a specific mission design was considered, in fact, regardless of the presence of reflective elements that can constitute a reflective telescope, all the concepts mentioned above present either a filter or a window or a lens and it is this first transmissive component linked to the cryostat or to the input port which was selected for this study.

In addition, all the optical elements considered in this context are always considered ideally thermally sinked at the edge and whilst for a ground cryostat several filters are needed to maintain a low radiative load, in space this is not needed due to reduced optical thermal loading.
Nevertheless, the adoption of large format array instruments leads to the usage of large optical elements, thus increasing their diameter, while preserving their thickness (defined by the thin film interference physics of the filter role). Consequently, even if the telescope design is optimized to reject stray light, effects due to delay in the transmission of thermal radiation and filters irradiation, will remain and could possibly increase.

This paper will focus on such issue by considering the amount of residual intensity irradiated by two types of polymer-based filters through a multiphysics [10] simulation. The satellite concept chosen was one of a probe spinning on its axis similarly to the Planck probe and equipped with a large format array of detectors with a large aperture. Specifically, the main CMB channels (100 and 143 GHz), where studied. Firstly, the filter parameters relevant to the simulation and its operation conditions will be described. Subsequently, a description on the physical properties of the materials involved and their parameters will be given. Finally, the simulations results will be pointed out.

II. FILTERS THERMAL MODEL

The filters studied in this paper are both considered to be made of polypropylene (PP) and specifically designed to have a peak transmission at 100 and 143 GHz. The only difference being the presence of a porous-polytetrafluoroethylene (pPTFE) coating that allows to shift the transmissivity maximum to 100 GHz. The geometry adopted for the simulation, as shown in Fig. 1, consists in a disk of 250mm radius and 4.9mm thick with a metal clamp at its edge to represent its mount and heat sink. When present, the pPTFE coating was assumed to be 625um thick.
With reference to such model, the heating equations and the material constants needed for the simulation were defined. The procedures adopted during these steps will be described in the following section.

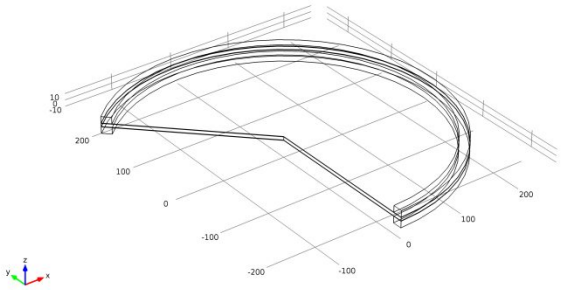

Figure 1: 3D image of a 100GHz filter, the axis scale is in mm.

A. Thermal model

Two mechanisms were considered to simulate heat transfer in solids: heat conduction and radiation transfer. The first one was modelled using the heat equation in the form of pure conductive heat transfer:

$$\rho C_p \frac{\partial T}{\partial t} + \nabla \cdot (-k\nabla T) = Q \tag{1}$$

where ρ is the material density, C_p the heat capacity at constant pressure, k the thermal conductivity and Q the total heat. Moreover, it should be pointed out that this form of the first law of thermodynamics was obtained from the general equation by ignoring viscous heating and pressure work and considering the velocity vector as null.
In addition to the effects caused by convection, radiative heating was considered. Its interaction with conductive heat transfer was described by adding a source term into the heat flux equation. By definition, this is equal to the difference between the incident radiation and the one leaving the surface. Nevertheless, since the material is not completely transparent, the interaction between medium and light was also considered.
In this case, three different kinds of interactions were taken into account: absorption, scattering and emission, which were included in the radiative heat transfer equation [11].

$$\mathrm{Q_R} = \Omega \cdot \nabla I(\Omega) = \kappa I_b(T) - \beta I(\Omega, s) + \frac{\sigma_s}{4\pi}\int_0^{4\pi} I(\Omega)\phi(\Omega', \Omega)\partial\Omega' \tag{2}$$

where $I(\Omega)$ is the radiative intensity at a given position, following the $I(\Omega)$ direction, while T, κ, β,σ_s are temperature, absorption, extinction and scattering coefficients, respectively. $I_b(T) = \frac{n^2\sigma T^4}{\pi}$ is the blackbody radiation with n refractive index of the media.
Finally, conductive heat transfer and radiative heat transfer were coupled by adding the heat flux term derived from equation (2) into the heat transfer equation. In this way a thermal multi-physics model was obtained and used to simulate the filters described above. Furthermore, the total equation was enhanced by adding a thorough

description of the thermal properties of PP and pPTFE as a function of temperature. Particularly, models for the thermal conductivity (k) and heat capacity (C_p) were obtained from data available in literature and from previous measurements [13], thus allowing to define variables such as their emissivity. The details about these models will be discussed in the following section.

B. Polymers physical properties

As introduced above, in order to address the heat transfer issue, a thermal model was required. In particular, equations for both heat capacity C_p and thermal conductivity k of PP and pPTFE were obtained from literature. Generally, in order to build a model for k and C_p of polymers one must take into account their dependence on temperature, cristallinity and orientation, which are different for each type of polymer considered. In fact, there are substantial distinctions in the values of thermal conductivity and heat capacity between amorphous, semi-crystalline and crystalline polymers, due to the diversity of their inner structure. This aspect has been exhaustively discussed in a number of papers [14-18] and they were also used in a recent study on the change of optical constants as a function of temperature [13]. In this context cryogenic data were obtained from literature for both PP [19, 20] and pPTFE [21, 22]. Figure 2 shows the curves of both quantities that were used in the thermal model.

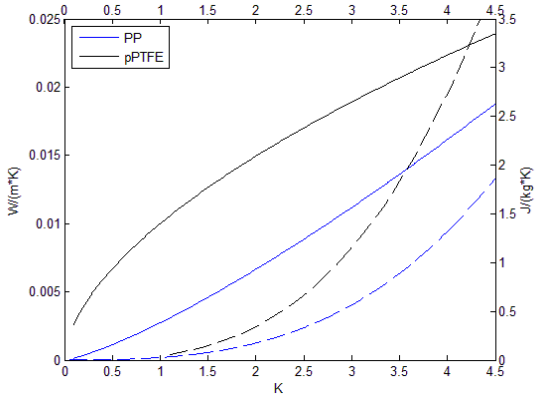

Figure 2: Materials thermal curves used in the simulation. The full lines show the thermal conductivity (left scale), while the dashed lines the heat capacity (right scale).

Moreover, equation (2) requires the optical properties of these materials to be computed properly. For this purpose, measurements from a previous experiment [13] together with data available from previous papers [22-24] were used to obtain the data relevant to the simulation from spectroscopy measurements. In such way it was possible to derive the figures of emissivity to be used in the simulation. For both polymers it was chosen to assign the value of $\alpha = \varepsilon = 0.01$ in the wavelength range of the experiment. In addition the numbers suggested that scattering values could be approximated to zero at the first order when operating at FIR or sub-mm frequencies.
Once these model were obtained, two different simulations were run, one for an uncoated polypropylene filter and one for a pPTFE coated, in a time interval of 60 minutes (60 satellite rotations). The results will be discussed in section 3.

C. Simulation definition

The simulation was performed using a Finite Element Analysis (FEA) software, COMSOL multiphysics [10]. For this purpose the 'Heat Transfer' module was used, since it allows to simulate heat transfer and radiation propagation at the same time.

Firstly, two heating sources were considered: the zodiacal light and Jupiter's thermal emission, being these the most likely dominant contributions in the Near to Mid-Infrared region. Zodiacal light model was based on the study performed for the EChO mission [12] and represented as superposition of the emission of two blackbodies, one at 5500K and one at 270K in the range $0.5 - 30\ \mu m$, whereas Jupiter's emission was simulated as a blackbody with a temperature of 140 K, in the same wavelength interval.

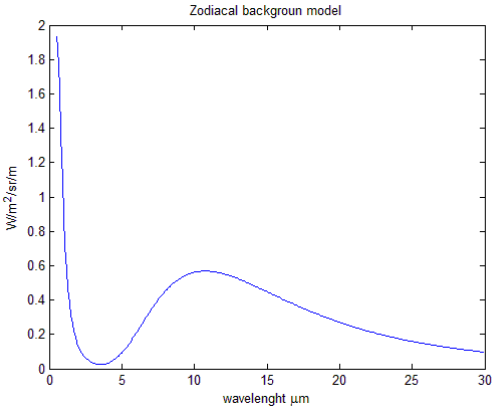

Figure 3: Representation of the zodiacal light model adopted in the simulation.

The integral of this curve multiplied by the filter throughput, was then used as the maximum amount of power incident on the filters (P_0), modulated by a function representing the satellite rotation and described with a sine wave term of same angular frequency. Moreover, it should be pointed out that this contribution should be seen as an upper limit, since the satellite rotation axis and the zodiacal signal are not necessarily co-aligned. In addition, this signal was taken not only due to its significant contribution but also as it behaves closer to a sine modulation than that of the galactic dust emission (in the NIR) which is closer to a one or two small peaks per rev. In this context, several cases were considered for the filter throughput $A\Omega$, basing on several instruments design proposed for CMB space missions[4,6,28] with values ranging from 0.3 to 900cm^{2}sr as shown in Table 1.
Finally, the FEA model was computed simulating a 60 min satellite run. Fig. 4 shows the schematics of the simulation settings, where the heat flux was set as a boundary condition at the top surface, whilst heat was propagated through conduction combined with radiative heat transfer. Proper boundary conditions were applied in order to control the radiation propagation by choosing the appropriate emissivity value each time. Finally in Table 1, some constants used in the simulation are listed.

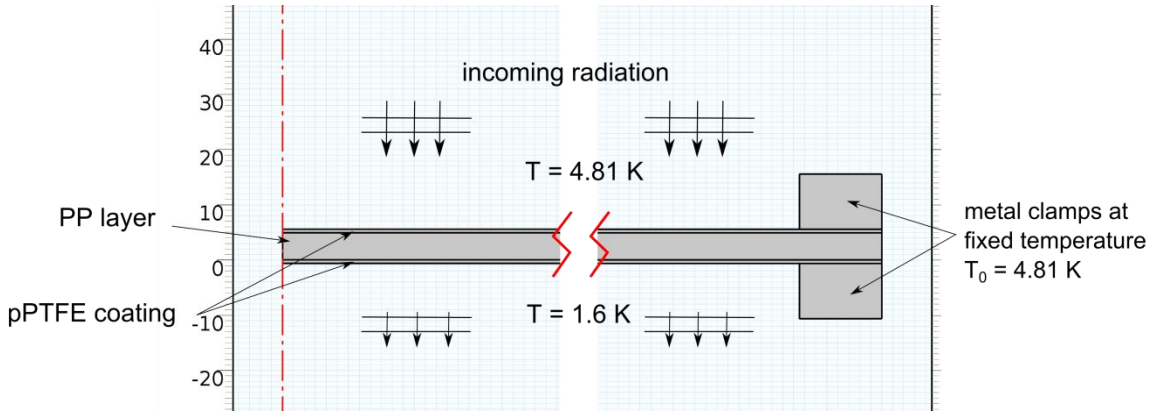

Figure 4: Conceptual scheme of the FEA simulation for a 100GHz filter. The 143GHz filter differs from the one shown here because of the absence of the pPTFE coating.

Incident power [W]	$A\,\Omega$ [cm^{2}sr]
$P_A = 1.0757 \cdot 10^{-4}$	0.3006
$P_B = 13 \cdot 10^{-4}$	3.6829
$P_{crs\_drg} = 0.2147$	600
$P_{epicIM} = 0.3220$	900

Table 1: Constants adopted in the FEA simulation

III. FILTERS HEATING

In this section, the simulation results will be summarized. Initially, two cases were identified, the ones where filters were thermalizing and the ones where they were not. In the first case temperature values from the top and bottom surface of the filter were used to fit a custom lumped model [26] which allowed to obtain the characteristics thermal constants. The equation used for the fit was the following:

$$T(t) = T_\infty + (T_0 - T_\infty)\mathrm{e}^{-t/\tau} - Asin(\omega t + \phi) \quad (3)$$

where T_∞ represents the equilibrium temperature, T_0 is the initial one and τ is the time constant of the problem. This function was modulated by a sinusoidal term which represents the periodic fluctuation due to the satellite rotation that causes a small, short-term variation, in the values of *T*. The phase term ϕ was introduced to take into account the difference in the *T* values between both surfaces due to the non-instantaneous heat propagation through the whole filter. Subsequently, for every representative value of temperature, the total transmitted energy was calculated using Planck's law in the 30% bandwidth frequency interval of the filter considered:

$$I = A\Omega \int_{0.85\nu_0}^{1.15\nu_0} \frac{2h}{c^2} \frac{\nu^3}{e^{h\nu/KT}-1} d\nu \quad (4)$$

where $A\Omega$ was obtained from the specifications used to calculate the incident intensity values and ν_0 was put equal to 100 and 143GHz for the pPTFE coated filter and for the uncoated one respectively. In this way the exact figures for the transmitted intensity were obtained for the considered wavelength bands.

Examples of the curves obtained from the simulations are shown in Fig. 5 and 6. The first one illustrates the different temperature values measured in the case of a low power load on the filters whilst the second one displays the figures from the high power simulations. In the former case it was possible to fit equation (3) to the data and obtain the characteristics numbers for each case considered. Table 2 lists the parameters calculated from the fits. It should be also pointed out that, since the quantities involved are representative, their value could change by 5-10% and the resulting fit figures would vary accordingly. For this reason, the numbers in Table 2 are given with a 1% precision.

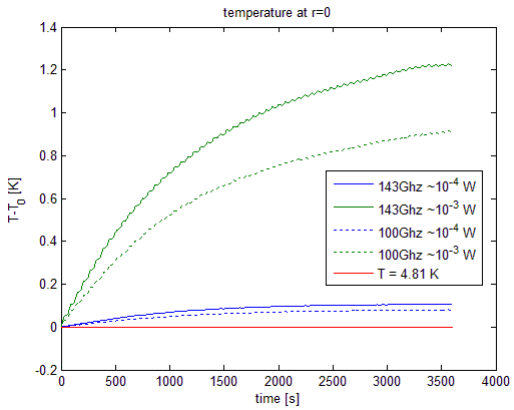

Figure 6: Temperature variation during the simulated time measured at the filter central point of the bottom surface, with incident power equal to 10^{-4} and 10^{-3} W.

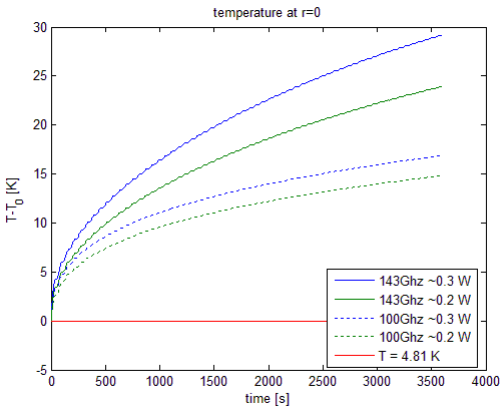

Figure 5: Temperature variation during the simulated time measured at the filter central point of the bottom surface, with incident power equal to 0.3 and 0.2 W.

	τ_{output} [s]	T_∞ [K]	$I(T_\infty)$[nW]	A[K]	ϕ
100 GHz P_A	1171	4.89510	8.0	0.00050	1.86
143 GHz P_A	1062	4.92210	18.3	0.00067	1.80
100 GHz P_B	1301	5.77490	125.9	0.00421	1.83
143 GHz P_B	1234	6.10140	327.2	0.00543	1.80

Table 2: Full list of the fit parameters obtained from the low power simulations. The values are obtained from the temperature at the output surface of the filters.

Overall it was observed that the filters where thermalizing only when the values of incident radiation where small. On the contrary, when the incident power was of the order of 10^{-1}W, a constant temperature was not reached.
In the first case, the fitted thermal time constants were of approximately 1000s. This was modulated by a smaller periodic oscillation due to the satellite rotation, which caused a change both in the phase term and the amplitude between the top and bottom surface. These differences were around 10^{-4} K with 10^{-4}W as incident intensity and 10^{-3} in the other case. Moreover, it was noticed that the value of T_∞ was higher for the uncoated filters compared to the pPTFE-coated ones, the difference being larger when the incident intensity was greater (case 10^{-3}W). On the contrary, greater time constants τ were found for the 100GHz filters.
Generally, all these effects were enhanced more when the input power was higher. In particular, it was noticed that, whilst the thermalization was reached only with low input power, the AC effect was present in all the cases studied. Finally, values of the transmitted intensity were calculated using the T_∞ figures from the fitted curves of the output surface temperatures. It was noticed that the filters showed a maximum emitted intensity of about 10nW in the *A* case and 100nW in the *B* one. Fig. 7 summarizes the values of temperature reached at the end of each simulation at the center of the output surface compared to the corresponding input power.

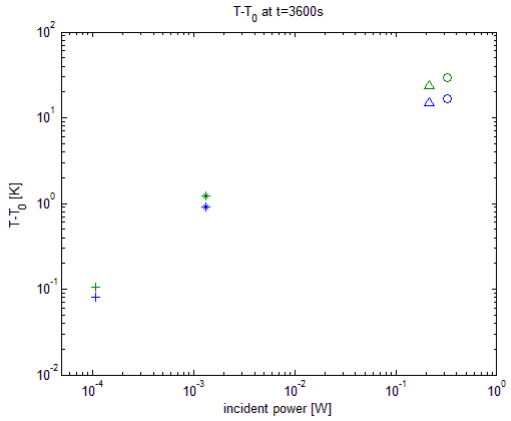

Figure 7: Temperature values measured at the bottom center of the filter for all the simulations at t=60min. The green points shows the numbers related to the 143GHz filters whilst the blue to the 100GHz ones.

Once these values were obtained, it was possible to find the equivalent CMB dipole amplitude that this effect would mimic (albeit with a different phase and orientation in the sky). This was done by minimizing the following equation:

$$I(T_\infty) = \int_{0.85\,\nu_0}^{1.15\,\nu_0} BB\left(T_{meas,\nu}\right) - BB\left(T_{cmb,\nu}\right) d\nu \qquad (5)$$

where $BB(T,\nu)$ represents the Planck's law. The results are listed in Table 3. It was found that this effect would be of 2mK in the worst case (higher incident power) and 0.1mK in the low power simulation. Potentially compromising a high-precision calibration (amplitude and alignment) on the CMB dipole.

Filter's central frequency	Incident power [W]	ΔT_{cmb} [mK]
100 GHz	$1.0757 \cdot 10^{-4}$	0.11
143 GHz	$1.0757 \cdot 10^{-4}$	0.11
100 GHz	$13 \cdot 10^{-4}$	1.76
143 GHz	$13 \cdot 10^{-4}$	2.02

Table 3: Temperature differences of T_{cmb} values calculated using (5).

IV. CONCLUSIONS

In this paper, it has been shown that polypropylene-based filters for FIR and sub-mm space applications present an increase in their temperature due to the heating from the incoming radiation. This was strongly depended on the throughput considered to be present at the input port, which allowed two different cases to be defined. When a larger incident power, of the order of 10^{-1}W was considered, the filters as they were designed did not thermalize and a steady increase in the temperature was observed. On the contrary, in the case when the incident radiation was around 10^{-3}W or lower, the increase was still observed but it allowed polypropylene to reach a constant value in temperature with characteristics time constants of $\sim$1000s. Particularly, the maximum deviation from the initial condition ($T_0 = 4.81$K) was equal to $\Delta T_{max} \sim 0.1$K in the P_A case and $\Delta T_{max} \sim 1.2$K in the P_B one.
In addition, small scale fluctuations due to the satellite rotation and consequent periodic variation of the incident intensity were preserved over time with amplitudes between 10^{-4} and 10^{-3}K, greater in the case of higher intensity. This effect was also observed in the high-power simulations and it remained present over the entire simulated period.

In addition, it should be pointed out that these results also depends on the model adopted to describe the polymers thermal properties, since a difference in the molecular structures would change the value of the constants used in the simulation. Nevertheless, this can be considered a second order effect since parameters like thermal conductivity and heat capacity vary less as the temperature decreases, because their structure properties become more similar [18].

Observations of an analogue effect was already measured in past space missions [27] where careful post-processing allowed its proper removal from science data. In fact if not removed, such effect would have caused extra flux density level to be present in the spectral images. Therefore, with increasing the size of the optics and thus filters, this would be enhanced enough to affect the measurement of objects that requires sensitivity of the order of few Jy in the Far-Infrared and sub-mm band. In this context, the knowledge of the optical and thermal properties of the materials which quasi-optical components are made is pivotal to thoroughly determine the order of magnitude of the effect described in this paper, thus allowing the design of a more precise instrument for cryogenic applications.

Finally, this work highlights the need for space instrument with large focal plane arrays to also employ thermal filters (thin film near-IR rejecting filters) before thick polymer optical elements, similarly to the ground-based systems. In fact, even in the thermalized case, their heating could alter the measurements of the CMB dipole temperature up to tens of percent together with shifting its spatial distribution out of phase.

ACKNOWLEDGMENTS

The research leading to these results has received funding from the European Union's Seventh Framework Programme (FP7/2007-2013) under FISICA grant agreement n. 312818.

REFERENCES

[1] G. L. Pilbratt, J. R. Riedinger, T. Passvogel, G. Crone, D. Doyle, U. Gageur, A. M. Heras, C. Jewell, L. Metcalfe, S. Ott, and M. Schmidt, "Herschel Space Observatory" *Astronomy and Astrophysics* 518, p. L1, July 2010.
[2] J. A. Tauber et al. "Planck pre-launch status: The Planck mission" *Astronomy and Astrophysics* 520, p. A1, Sept. 2010.
[3] T. Nakagawa, H. Matsuhara, and Y. Kawakatsu, "The next-generation infrared space telescope SPICA" *SPIE Space Telescopes and Instrumentation* 8442, p. 84420O, Aug. 2012.
[4] J. Bock, A. Cooray, S. Hanany, B. Keating, A. Lee, T. Matsumura, M. Milligan, N. Ponthieu, T. Renbarger, and H. Tran, "The Experimental Probe of Inflationary Cosmology (EPIC): A Mission Concept Study for NASA's Einstein Inflation Probe," May 2008.
[5] "B-Pol Mission." http://www.b-pol.org/index.php
[6] P. Andre et al. "PRISM (Polarized Radiation Imaging and Spectroscopy Mission): A White Paper on the Ultimate Polarimetric Spectro-Imaging of the Microwave and Far-Infrared Sky," tech. rep., June 2013.
[7] P. a. R. Ade, G. Pisano, C. Tucker, and S. Weaver, "A Review of Metal Mesh Filters," in *SPIE Millimeter and Submillimeter Detectors and Instrumentation for Astronomy*, 6275, pp. 62750U–62750U–15, June 2006.

[8] C. E. Tucker and P. a. R. Ade, "Thermal Filtering For Large Aperture Cryogenic Detector Arrays," in Proc. *SPIE 6275, Millimeter and Submillimeter Detectors and Instrumentation for Astronomy III*, pp. 62750T-62750T-9, June 2006.
[9] A. Catalano et al. "Characterization and Physical Explanation of Energetic Particles on Planck HFI Instrument," Mar. 2014.
[10] "Comsol multiphysics" http://www.comsol.com/.
[11] M. Modest, Radiative Heat Transfer, *Academic Press*, 2nd ed., 2003.
[12] "Echo mission requirements." http://sci.esa.int/jump.cfm?oid=51293.
[13] N. Baccichet, G. Savini, P. A. R. Ade, and P. Hargrave, "Detailed Characterization of the optical constants of polymers as a function of temperature," in 35th ESA Antenna Workshop, 2013.
[14] G. J. Morgan and D. Smith, "Thermal conduction in glasses and polymers at low temperatures" *Journal of Physics C: Solid State Physics* 7, pp. 649–664, 1974.
[15] S. Burgess and D. Greig, "The low-temperature thermal conductivity of polyethylene" *Journal of Physics C: Solid State Physics* 8, pp. 1637–1648, 1975.
[16] C. L. Choy, "Thermal conductivity of polymers," *Polymer Engineering & Science* 18, pp. 984–1004, 1977.
[17] C. L. Choy and D. Greig, "The low temperature thermal conductivity of isotropic and oriented polymers" *Journal of Physics C: Solid State Physics* 169(10), pp. 169–179, 1977.
[18] C. L. Choy and K. Young, "Thermal conductivity of semicrystalline polymers - a model" *Polymer Engineering & Science* 18, pp. 769–776, 1977.
[19] M. Barucci, E. Gottardi, E. Olivieri, E. Pasca, L. Risegari, and G. Ventura, "Low-temperature thermal properties of polypropylene" *Cryogenics* 42, pp. 551–555, Sept. 2002.
[20] E. D. Marquadrt, J. P. Le, R. Radebaugh, "Cryogenic Material Properties Database" *11 International Cryocooler Conference*. 2000.
[21] W. Reese and J. E. Tucker, "Thermal Conductivity and Specific Heat of Some Polymers between 4.5 and 1K" *The Journal of Chemical Physics* 43(1), p. 105, 1965.
[22] D. J. Benford, M. C. Gaidis, and J. W. Kooi, "Optical properties of Zitex in the infrared to submillimeter" *Applied optics* 42, pp. 5118–22, Sept. 2003.
[23] G. W. Chantry, J. W. Fleming, P. M. Smith, M. Cudby, and H. A. Willis, "Far Infrared and millimetre-wave absorption spectra of some low-loss polymers" *Chemical Physics Letters* 10(4), pp. 473–477, 1971.
[24] J. Birch, "The far-infrared optical constants of polypropylene, PTFE and polystyrene," Infrared Physics 33, pp. 33–38, Jan. 1992.
[25] J. Zhang, P. a R Ade, P. Mauskopf, G. Savini, L. Moncelsi, and N. Whitehouse, "Polypropylene embedded metal mesh broadband achromatic half-wave plate for millimeter wavelengths" *Applied optics* 50, pp. 3750–7, July 2011.
[26] F. P. Incropera, D. P. DeWitt, T. L. Bergman, and A. S. Lavine, Fundamentals of Heat and Mass Transfer, John Wiley & Sons, 2006.
[27] B. M. Swinyard et al. "In-flight calibration of the Herschel -SPIRE instrument" *Astronomy and Astrophysics* 518, p. L4, July 2010.
[28] M. D. Niemack, personal communication. Contact: niemack@cornell.edu